Received: 10 August 2018 | Revised: 24 October 2018 | Accepted: 2 November 2018

DOI: 10.1002/adv.22155

RESEARCH ARTICLE

WILEY

Polymer–spinel ferrite composite containing nickel, magnesium, and nickel–magnesium ions: Structural, magnetic, electrical, and thermal stability properties

Emad M. Masoud | **Abdelhameed A. El-Bellihi** | **Wafaa A. Bayoumy** | **Amira S. Abdallah**

Chemistry Department, Faculty of Science, Benha University, Benha, Egypt

Correspondence
Emad M. Masoud, Chemistry Department, Faculty of Science, Benha University, Benha, Egypt.
Emails: emad.youssef@fsc.bu.edu.eg; emad_masoud1981@yahoo.com

Funding information
Benha University

Abstract

Firstly, three different nano ferrites ($MgFe_2O_4$, $NiFe_2O_4$, and $Ni_{0.5}Mg_{0.5}Fe_2O_4$) were synthesized using a combustion method. Secondly, polyaniline composites containing small amounts of those nano ferrites were prepared using in situ chemical polymerization method. Ferrite samples were characterized using X-ray diffraction (XRD) and Fourier transform infrared spectroscopy (FT-IR) analyses. XRD analysis of ferrites exhibited well-resolved broad peaks, which confirm the polycrystalline and mono-phasic nature. FT-IR confirmed the spinel structure of these ferrites. Polymer nano ferrites composites were also characterized using XRD, FT-IR, thermal analysis (TG and DTA), and transmission electron microscope (TEM). Also, electrical (AC conductivity, dielectric constant, dielectric loss, and complex impedance) and magnetic properties were investigated for all nano composite samples. XRD analysis confirmed the formation of polymer nano composites. Moreover, the absorption bands of polyaniline were shifted in the presence of the three different ferrites, confirming the presence of interactions between the different phases in all composites. Additionally, different thermal stability behavior of nano composite samples was observed, which may be attributed to the nano ferrite type and the physical interactions nature with polymer matrix. The sample containing nano magnesium ferrite showed the core–shell structure by TEM. The same sample exhibited the highest values of both AC conductivity (1.01×10^{-4} ohm^{-1} cm^{-1}) and magnetization saturation (3.38 emu/g) at room temperature. In comparison with other similar composites containing large amounts of the same ferrite, the investigated sample showed a good magnetization saturation value and thermal stability behavior.

KEYWORDS

core–shell structure, electrical properties, magnetic properties, polymer nano ferrite composites

1 | INTRODUCTION

Polymer nano composites with electrical properties, incorporated with inorganic magnetic oxides, have attracted obvious interest as of their potential applications for combining properties that are difficult to attain separately with the individual components.[1] The basic idea in a composite is to collect several materials and their properties in a single one.[2] The magnetic properties with the conductive ones lead to producing new materials such as conductive polymers with a magnetic behavior, or magnetic particles having a conductive polymer.[3] Also, these materials have potential applications such as microwave absorption, batteries, electrochemical display devices, and electrical–magnetic shields.[4–9]

Intrinsic conducting polymers, as polyaniline, are a novel class of synthesized materials having the electrical and optical properties of semiconductors and metals, in addition to the mechanical ones. Also, a high level of conductivity can be achieved in intrinsic conducting polymers through oxidation–reduction and doping with a suitable dopant.[10] The reasons for making those polymers are popular basic materials for advanced applications.[11] It is well known that polyaniline and its derivatives can be considered as the most promising conducting polymer as of its unique electrical, optical, and opto-electrical properties, its straightforward and easy polymerization, in addition to its excellent environmental stability.[11] In contrast, spinel ferrites of the type MFe_2O_4 (M is a divalent metal cation) are currently the key materials for advancements in electronics, magnetic storage, and ferro-fluid technology.[12] In our present work, we aimed to synthesize a novel nano composite with good magnetic and conductive properties, which are difficult to be combined together. We chose to combine the intrinsic conducting polyaniline (PAn) with three different ferrites, $MgFe_2O_4$, $NiFe_2O_4$, and $Mg_{0.5}Ni_{0.5}Fe_2O_4$, due to the specific and unique properties of each. These ferrites and others were previously used many times with polyaniline. According to the literature survey, the important notice was that the used amounts of ferrites were high.[13–15] It is well known that the large ferrite amount can positively affect the magnetization saturation (M_s) value. In contrast, some properties such as electrical and mechanical ones will be negatively affected. In this vein, our new aim was to combine small amount of magnetic material with polyaniline, to get more enhanced electrical and magnetic properties and keep other ones. Additionally, this idea will be performed using three different ferrites with the same concentration, to compare their abilities to physically interact with the polymer matrix, and to finally determine which small amount can achieve the optimized values. A comparison of previous studies reporting a large amount of ferrites will also be studied.

2 | EXPERIMENTAL WORK

2.1 | Preparation of nano ferrites

Mg $(NO_3)_2$ [99%, Merck], Ni $(NO_3)_2$ [99%, Sigma-Aldrich], Fe $(NO_3)_3$ [99%, Merck], and urea [99%, Sigma-Aldrich] were used as received without purification to synthesize the nano ferrites ($MgFe_2O_4$, $NiFe_2O_4$, and $Mg_{0.5}Ni_{0.5}Fe_2O_4$). These nano ferrites were synthesized by a combustion process. In this method, and for each nano ferrite, a desired amount of nitrates and apparently estimated amount of urea, used as the fuel, were dissolved in distilled water until a homogeneous solution resulted. Following, the homogeneous solution was heated to dryness at 90°C, and then, the dried mass was calcined at 700°C for 2 hr, to finally obtain the nano ferrite.

2.2 | Preparation of polyaniline nano composites

In situ chemical polymerization method was used to prepare the polyaniline nano composites.[16] 0.25 g (13 wt.% of aniline) of each ferrite was added to 100 ml of a solution containing 0.2 M aniline in 1 M HCl. Following, 100 ml of a solution containing 0.25 M ammonium persulfate was added in drops to the acidic aniline solution while stirring at 25°C for 12 hr. The polyaniline nano composite was separated on a filter paper, washed with deionized water and acetone, and then dried at 90°C in an electrical oven.

Pure and three nano composite samples were prepared. The samples were denoted as PAn (pure polyaniline), PMF (polyaniline containing 13 wt.% of magnesium ferrite, PAn/$MgFe_2O_4$), PNF (polyaniline containing 13 wt.% of nickel ferrite, PAn/$NiFe_2O_4$), and PMNF (polyaniline containing 13 wt.% of magnesium–nickel ferrite, PAn/$Mg_{0.5}Ni_{0.5}Fe_2O_4$).

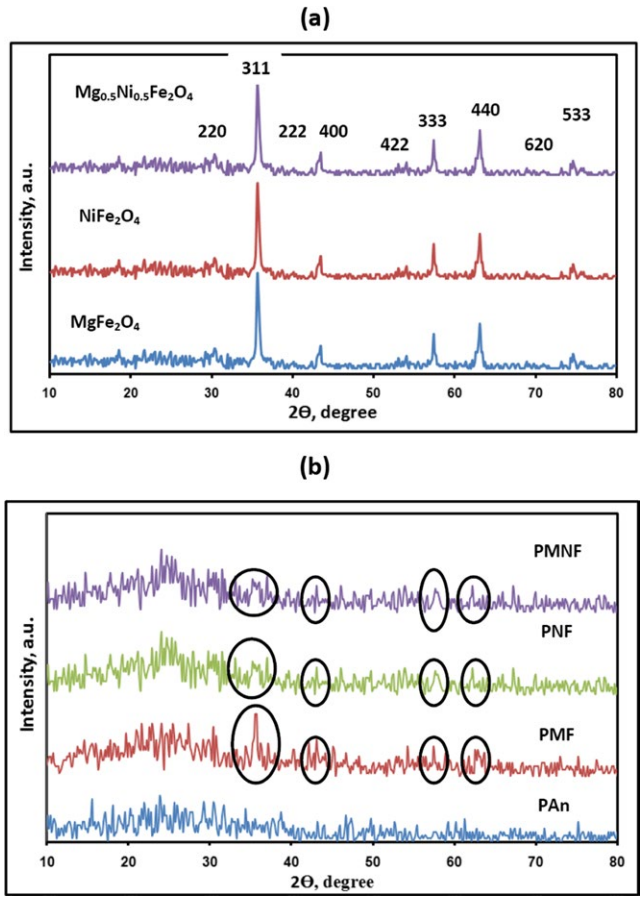

FIGURE 1 X-ray diffraction patterns of (a) $MgFe_2O_4$, $NiFe_2O_4$, $Mg_{0.5}Ni_{0.5}Fe_2O_4$ and (b) PAn, PMF, PNF, PMNF

2.3 | Characterization

X-ray diffraction analysis was performed on a Diano (made by Diano Corporation, USA). The pattern was run with Cu-filtered CuKα radiation ($\lambda = 1.5418$ Å) energized at 45 kV and 10 mA. The samples were measured at a room temperature in a range from $2\theta = 10°$ to 80°. The infrared spectra of the samples were recorded in the range of 4,000–400 cm^{-1} using a Bruker–FT-IR. TG and DTA were performed in a nitrogen atmosphere with a constant heating rate of 10 K/min in a temperature range of 298–873 K using Shimadzu DT-50. The morphology was analyzed using transmission electron microscope (TEM) operating at an accelerating voltage of 200 kV (JEOL, JEM 2100F). The electrical conductivity measurements were performed by sandwiching the powder samples (tablets) between two stainless steel electrodes using a programmable automatic LCR bridge (Model RM 6306 Phillips Bridge) in various temperatures ranging from 298 to 378 K. The magnetic properties were measured using a vibrating sample magnetometer (VSM; Lake Shore 7404).

3 | RESULTS AND DISCUSSION

3.1 | X-ray diffraction analysis

X-ray diffraction patterns of ferrites ($MgFe_2O_4$, $NiFe_2O_4$, and $Mg_{0.5}Ni_{0.5}Fe_2O_4$) are shown in Figure 1a. All patterns consist of well-resolved broad peaks, which confirm the polycrystalline and mono-phasic nature of the prepared ferrites. The diffraction peaks corresponded to planes of (2 2 0), (3 1 1),

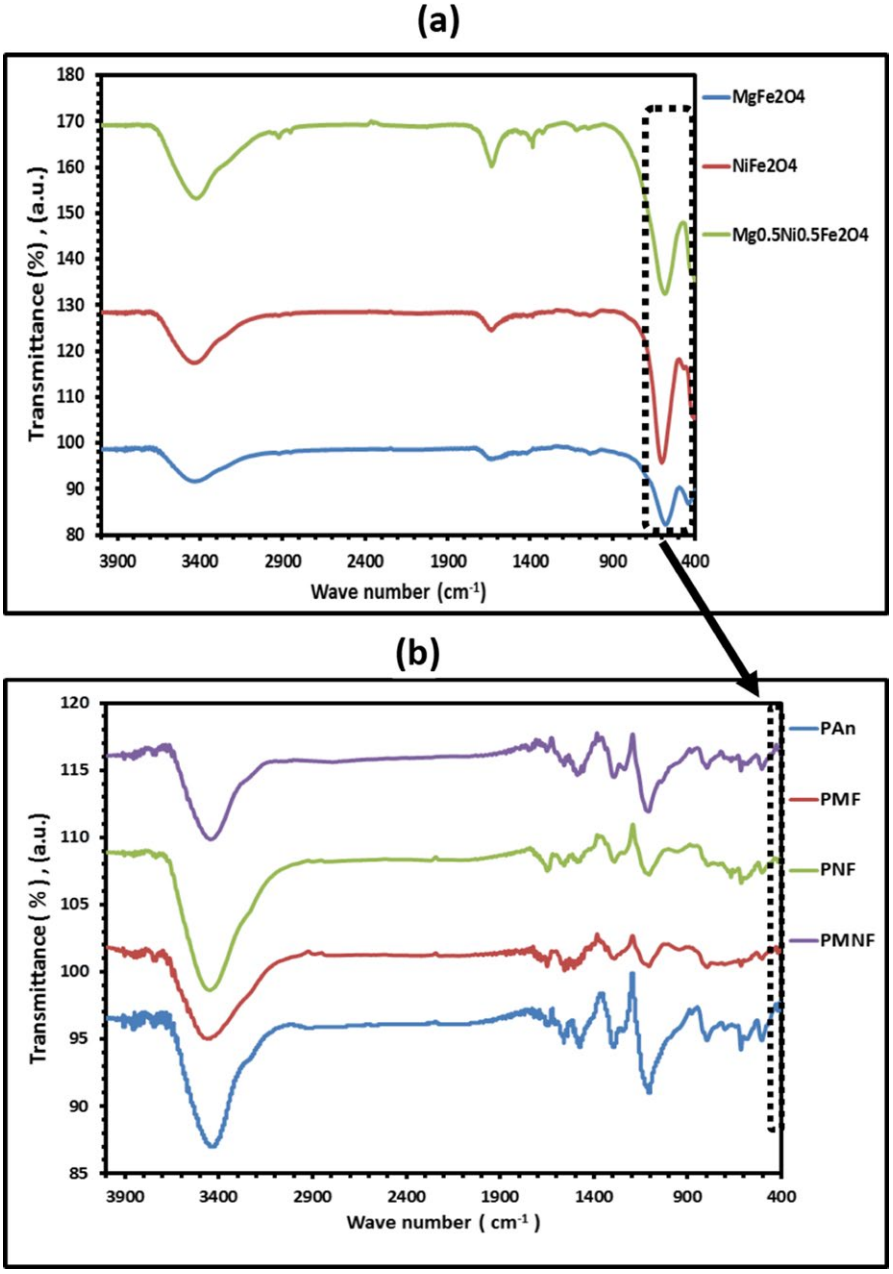

FIGURE 2 Fourier transform infrared patterns of (a) $MgFe_2O_4$, $NiFe_2O_4$, $Mg_{0.5}Ni_{0.5}Fe_2O_4$ and (b) PAn, PMF, PNF, PMNF

(2 2 2), (4 0 0), (4 2 2), (3 3 3), (4 4 0), (6 2 0), and (5 3 3) provide a clear evidence for the formation of a single-phase spinel structure of ferrite.[17] According to ICDD card number (73-1720) and JCPDS (73-2410) file of $MgFe_2O_4$ sample, as an example, the single-phase spinel structure was also confirmed. The average crystallite size of all ferrites was calculated using Scherer equation[18] and found equals 13, 6, and 26 nm for $MgFe_2O_4$, $NiFe_2O_4$, and $Mg_{0.5}Ni_{0.5}Fe_2O_4$, respectively. Additionally, the X-ray diffraction patterns of PAn, PMF, PNF, and PMNF samples are also shown in Figure 1b. The pattern of PAn shows the amorphous structure in addition to a broad diffraction peak at 2θ value of 25.3°, which corresponds to the periodicity parallel and perpendicular to the polymer chains, respectively.[19] On the other hand, the patterns of polymer nano ferrites composites show the pure ferrite crystalline peaks, but with low intensity, as represented by circles on the figure. This may be attributed to the small amounts of ferrites (only 13 wt.%) incorporated in the polymer matrix. Meanwhile, as no new crystalline peaks are observed, the X-ray diffraction analysis confirms the polymer nano ferrites composite formation.

3.2 | FT-IR analysis

The FT-IR spectra of both pure ferrites and polymer nano ferrite composites are shown in Figure 2a,b. Firstly, for the spectra of pure ferrites ($MgFe_2O_4$, $NiFe_2O_4$, and $Mg_{0.5}Ni_{0.5}Fe_2O_4$), the band at 3,470 cm^{-1} is attributed to the stretching vibrations of the hydrogen-bonded OH groups.[20] The bands over the range of 1,000–400 cm^{-1} (570, 460 cm^{-1}) correspond to metal–oxygen bond (Mg and/or Ni–O and Fe–O stretching) vibrations of the spinel structure compound[20] that was already confirmed by XRD (Figure 1a). Secondly, for the spectra of PAn, PMF, PNF, and PMNF, the main observed bands of PAn at 3,419, 1,560/1,475, 1,290, and 1,128 cm^{-1} are corresponding to N–H stretching vibration, C=C stretching vibration of quinine ring and benzene (B) ring, N–H bending stretching of benzenoid ring, and C–H in-plane bending vibration, respectively.[21] To also investigate the expected interactions between the metal oxides (nano ferrites) and PAn, the interpreted absorption bands of PAn were investigated in the nano ferrite composites. It was found that all absorption band values of PAn were shifted, in general, to higher ones. This indicates the interactions existing between the metal oxides and PAn matrix. All shifted values were tabulated in Table 1. Additionally, the same thing was observed for the absorption band values of metal oxides (570, 460 cm^{-1}). These values were also shifted, but to lower ones as obviously shown in Figure 2b.

3.3 | Thermal analysis

To investigate the thermal stability of PAn and polymer nano ferrites composites (PMF, PNF, and PMNF), thermal

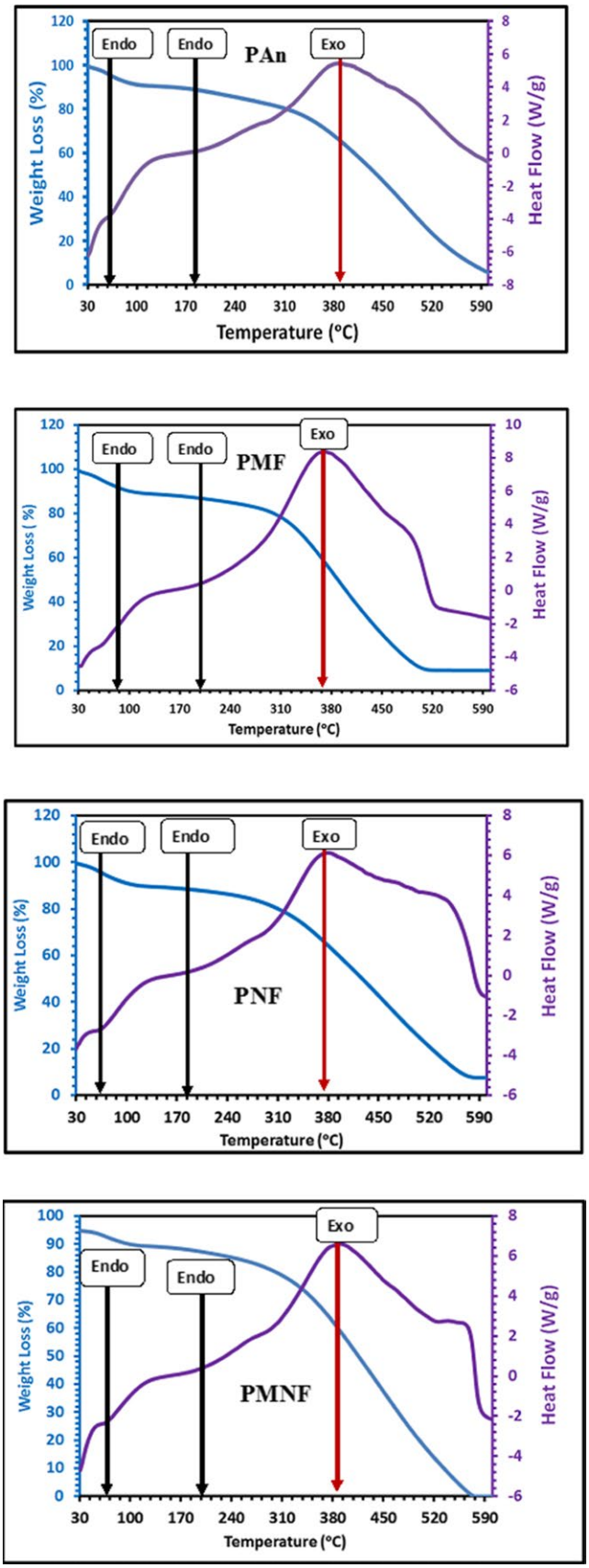

FIGURE 3 Thermal analysis patterns (TG and DTA) of PAn, PMF, PNF and PMNF samples

TABLE 1 FT-IR spectral basic bands assignment of PAn, PMF, PNF and PMNF samples.

PMNF	PNF	PMF	PAn	Wave number (cm^{-1})
3429	3423	3425	N-H stretching vibration	3419
1571	1566	1569	C=C stretching vibration of quinine ring and benzene (B) ring	1560/1475
1294	1289	1299	N-H bending stretching of benzenoid ring	1290
1134	1131	1135	C-H in- plane bending vibration	1128

analyses (TG and DTA) were performed and shown in Figure 3. The figure showed three main steps of decomposition for all investigated samples. The first decomposition step (up to 120°C) is due to the expulsion of water molecules and the dopant HCl from PAn chains,[2] this decomposition was also confirmed through DTA curve, as endothermic peaks (at ~62, 87, 70, and 76°C for PAn, PMF, PNF, and PMNF, respectively, as shown in Figure 3) were observed. The second weight loss step (from around 140 to 300°C) may be attributed to the volatilization of lower weight PAn. This volatilization was also confirmed through DTA, as endothermic peaks (at ~187, 200, 187, and 200°C for PAn, PMF, PNF, and PMNF, respectively, as shown in Figure 3) were observed. The final third step at higher temperatures can be attributed to the destruction of the polymer backbone[2] which was also confirmed through DTA, as exothermic peaks (at ~387, 360, 375, and 385°C for PAn, PMF, PNF, and PMNF, respectively, as shown in Figure 3) were observed. Additionally, it was observed that the weight of each sample becomes stable at a definite temperature. This means that the investigated samples have different thermal stability. Furthermore, this also shows that the small incorporated amounts of nano ferrites have interactions with the polymer matrix chains. The temperature values of weight loss stability were determined as 600, 512, 575, and 575°C for PAn, PMF, PNF, and PMNF, respectively. This reveals that the samples containing the small nano ferrites have a near-thermal stability value to the pure one, and the PMF sample has the lowest value (512°C).

3.4 | TEM analysis

The morphology was also studied to investigate the difference between pure and nano ferrite composite samples as

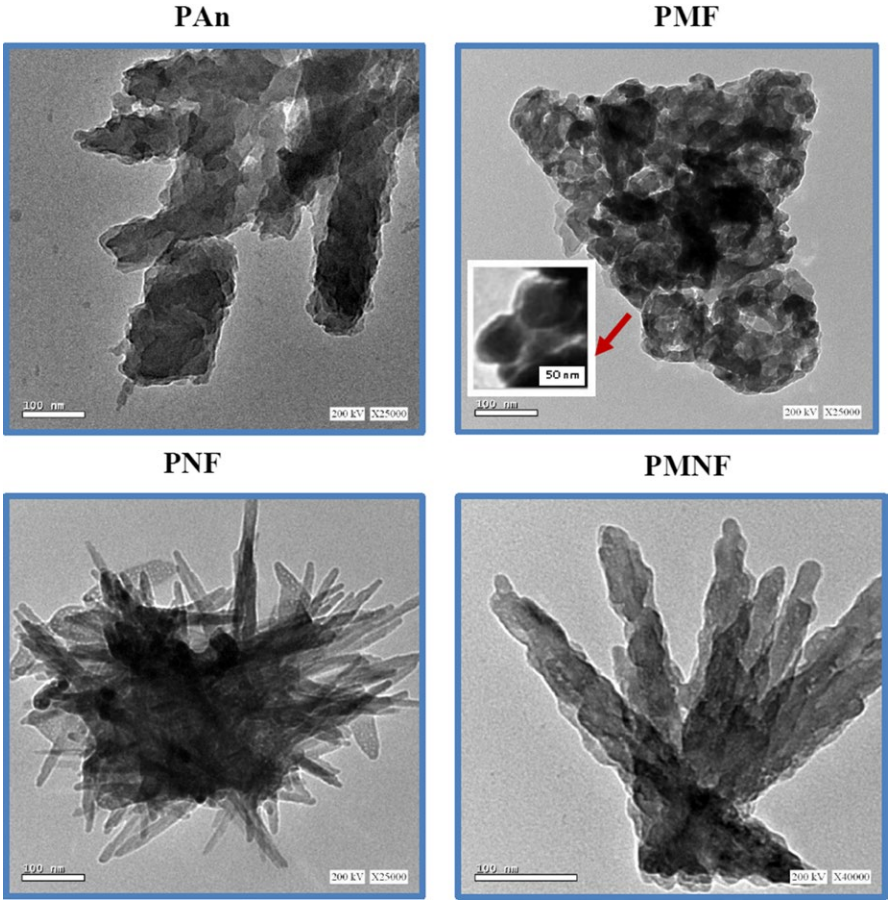

FIGURE 4 Transmission electron microscope patterns of PAn, PMF, PNF and PMNF samples

shown in Figure 4. The figure showed three different morphologies: agglomeration of irregular particles for PAn sample, agglomeration of particles having an interesting core–shell structure for PMF sample, and agglomeration of particles having rod shape for PNF and PMNF samples. It is well known that the particle shape depends on more than one factor, such as preparation method, conditions, concentration, and structure (ionic radius, surface charge, etc). As we here have the same preparation method, conditions, and also concentrations, so we think that the different structure nature (ionic radius, surface charge, etc) will play the biggest role in determining the nuclei growth rate and its direction during the preparation method to finally have more and more suitable energy with a stable texture. For this reason, we can get different shapes (rods, irregular, and core–shell) for the different nano ferrites.

For the core–shell structure of PMF particles, the magnification inset (Figure 4) shows a dark core and a light shell. The dark core represents the nano ferrite particles ($MgFe_2O_4$), and the light-colored shell represents the PAn. To further illustrate the formation of the core–shell structure through the chemical polymerization of PAn in the presence of $MgFe_2O_4$ particles, a Scheme 1 was added. As it is well known, the surface charge of the metal oxide is positive in acidic mediums. An amount of Cl^- ions are adsorbed on the nano ferrite surface to compensate the positive charges. In the same acidic medium, the aniline monomers as described converted to cationic anilinium ions, and as a result, electrostatic interactions produced between the adsorbed anions and cationic anilinium ions are described in Scheme 1.

3.5 | Electrical conductivity properties

The temperature dependence of AC conductivity was studied at 5 MHz for PAn, PMF, PNF, and PMNF as shown in Figure 5. Obviously, the figure shows that the presence of small nano ferrite amounts enhanced the AC conductivity of the PAn sample. This can be attributed to the small nano ferrite amounts that can induce a more efficient network formation for charge transport in the base PAn–matrix, resulting in

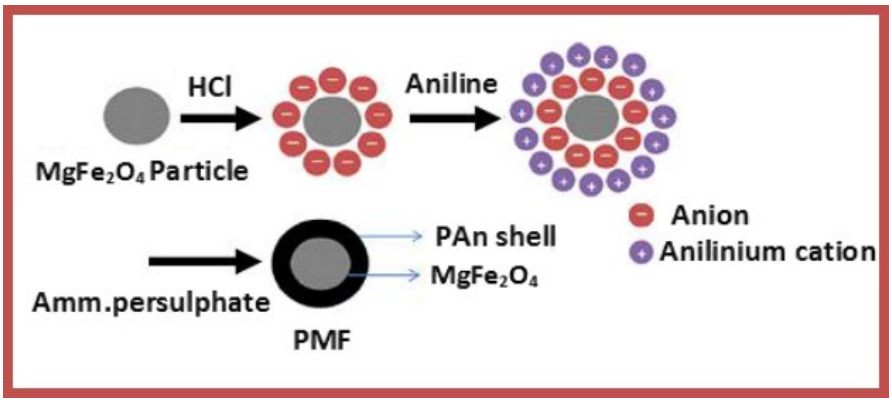

SCHEME 1 Synthesis of PMF composite

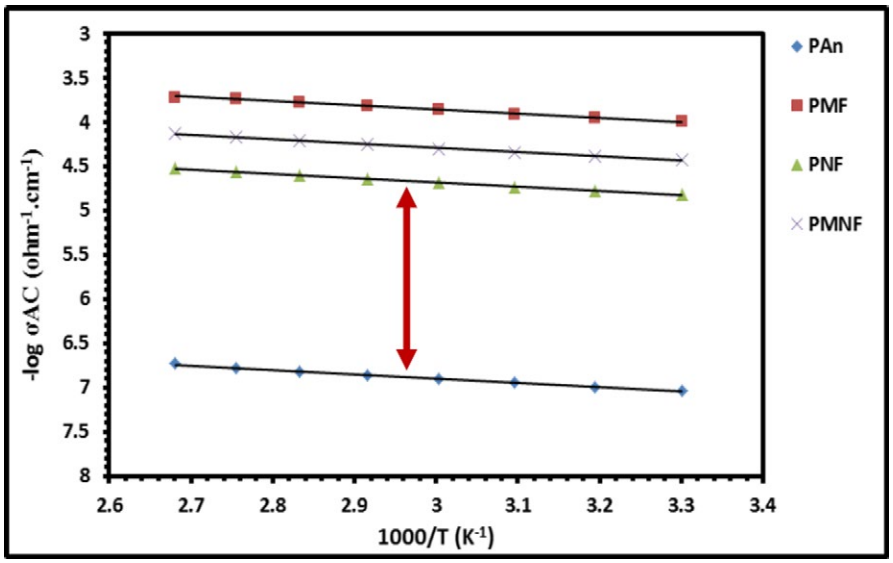

FIGURE 5 Temperature dependence of AC-conductivity of PAn, PMF, PNF and PMNF samples at 5 MHz

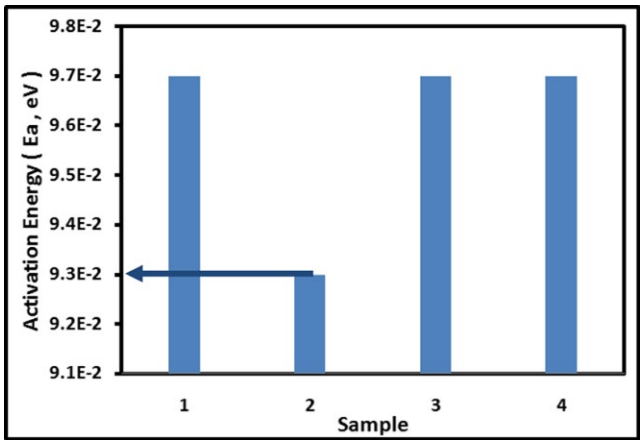

FIGURE 6 Activation energy values of 1: PAn, 2: PMF, 3: PNF and 4: PMNF samples

high conductivity values.[22,23] The efficient network formation in the presence of ferrites is originated from the additionally generated extended states and charged defects with electronic structures. This efficient network can be discussed in the light of interchain hopping mechanism; the electrical conductivity of conducting polymers results from mobile charge carriers introduced into the π-electronic system through composite formation (doping). At low concentrations, these charge carriers are self-localized and form nonlinear configurations. Because of large interchain transfer integrals, the transport of charge is believed to be principally along the conjugated chains, with interchain hopping as a necessary secondary condition.[24–27] The PMF sample exhibited the highest conductivity value ($\sigma_{AC} = 1.01 \times 10^{-4}$ ohm^{-1} cm^{-1}) compared to the other ones as in the following conductivity order: PMNF, $\sigma_{AC} = 3.72 \times 10^{-5}$ ohm^{-1} cm^{-1} > PNF, $\sigma_{AC} = 1.51 \times 10^{-5}$ ohm^{-1} cm^{-1}.

Here, it is worthwhile to mention that the PMF sample having the interesting core–shell structure (as confirmed by TEM in Figure 4) exhibits the highest electrical conductivity. This also may be attributed to the core–shell structure which can induce the most efficient PAn network (extended states and charged defects with electronic structures), and, as a result, a high conductivity. Figure 5 also shows that AC conductivity increases upon increase in temperature for all investigated samples. This behavior can be described by Arrhenius formula[28]

$$\sigma_{AC} = \sigma_0 \exp.(-E_{AC}/kT) \quad (1)$$

where σ_0 is a temperature-independent term, k is the Boltzmann constant, T is the absolute temperature, and E_{AC} is the apparent activation energy. Figure 6 represents the activation energy values. The figure showed that the PMF sample has the lowest one (0.093 eV) compared to the other ones. All values are also tabulated in Table 2.

3.6 | Dielectric constant

Dielectric constant (ε') versus temperature (at 5 MHz) and frequency (at 303 K) were studied for PAn, PMF, PNF, and PMNF as shown in Figures 7 and 8. Firstly, for the temperature dependence of dielectric constant, all samples

TABLE 2 Values of AC-conductivity and activation energy of PAn, PMF, PNF and PMNF samples.

Sample	AC-conductivity at 303 K, ohm^{-1}·cm^{-1}	Activation Energy (E_a,ev)
PAn	9.21×10^{-8}	0.097
PMF	1.01×10^{-4}	0.093
PNF	1.51×10^{-5}	0.095
PMNF	3.72×10^{-5}	0.094

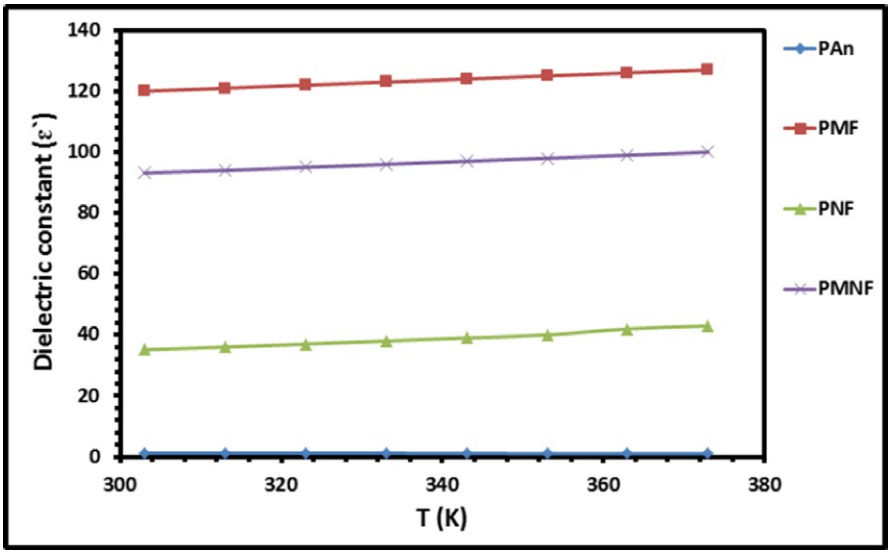

FIGURE 7 Temperature dependence of dielectric constant of PAn, PMF, PNF and PMNF samples at 5 MHz

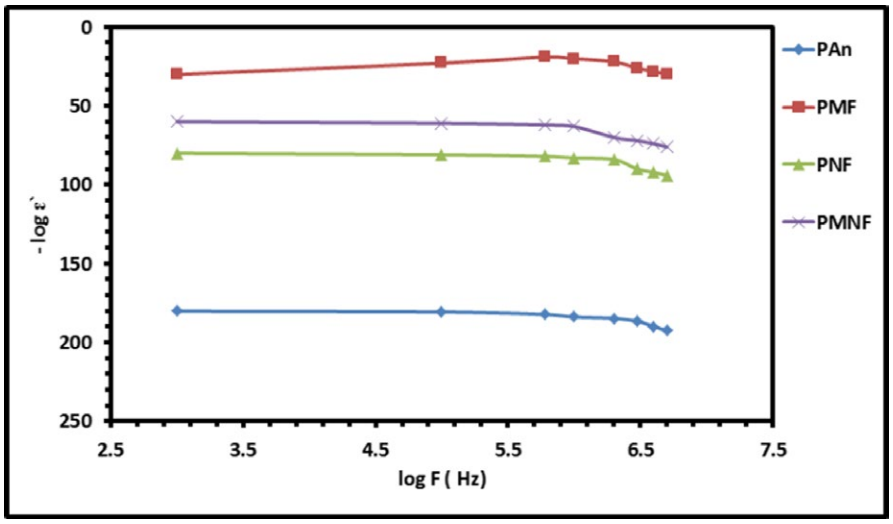

FIGURE 8 Frequency dependence of dielectric constant of PAn, PMF, PNF and PMNF samples at room temperature (303 K)

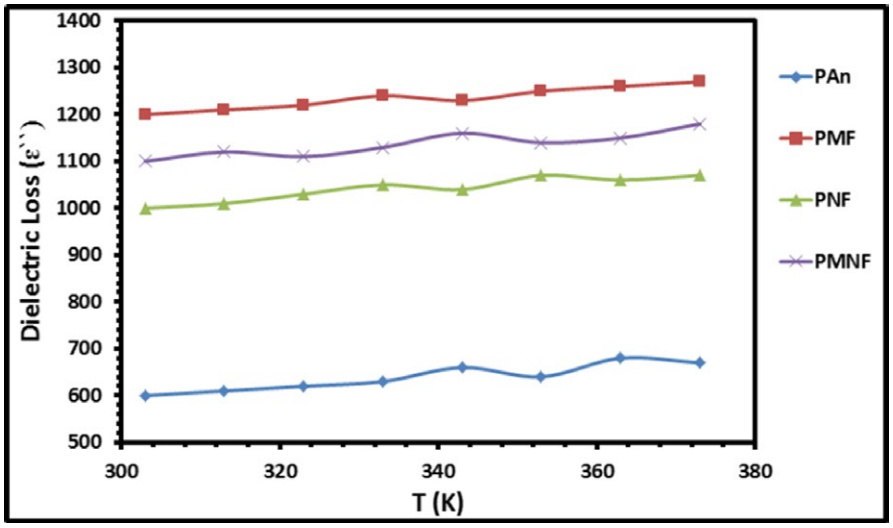

FIGURE 9 Temperature dependence of dielectric loss of PAn, PMF, PNF and PMNF samples at 5 MHz

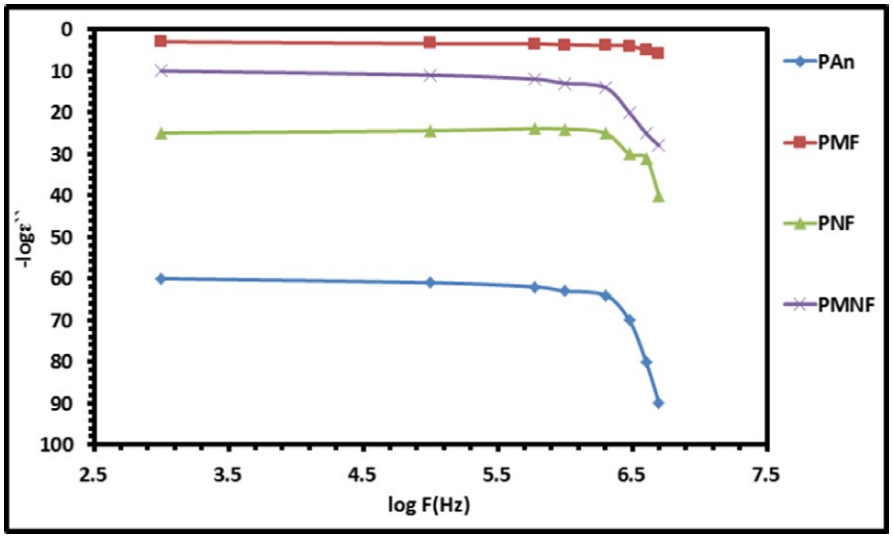

FIGURE 10 Frequency dependence of dielectric loss of PAn, PMF, PNF and PMNF samples at room temperature (303 K)

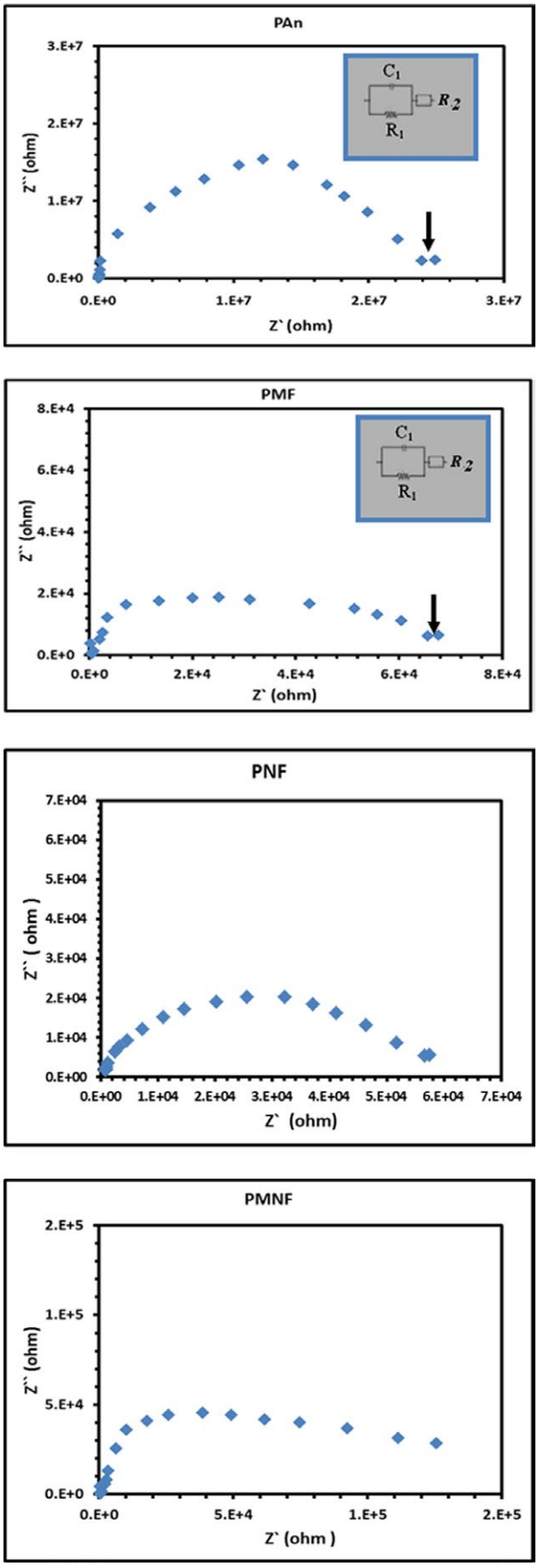

FIGURE 11 Complex impedance of PAn, PMF, PNF and PMNF samples at room temperature (303 K)

showed an increase in dielectric constant with an increase in temperature. This can be explained on the basis that as the temperature increases, the thermal energy librates more localized dipoles and the field tries to align them in its direction.[29–36] At the same time, the PMF sample having the core–shell structure exhibited the highest values of dielectric constant compared to the other ones. The sample showed a value of 110, while the others showed the following value order: PMNF, 93.2 > PNF, 35.2 > PAn, 1.2, at 303 K. The dielectric properties of these samples are mainly due to interfacial polarization process[37–44] and intrinsic electric dipole one[45] which all are partially attributed by the disordered motion of the charge carrier along the backbone of conducting polymer chain. Secondly, the frequency dependence of dielectric constant showed a decrease in behavior through two ranges, the first (at a frequency between 1 KHz and 1 MHz) exhibited a weakly dependent behavior and the second (at a frequency between 2 and 5 MHz) exhibited a strong one. Additionally, all values order of dielectric constant at 1 KHz comes as the same of the temperature dependence. The PMF sample showed a value of 110.

3.7 | Dielectric loss

Dielectric loss (ε'') versus temperature (at 5 MHz) and frequency (at 303 K) were studied for PAn, PMF, PNF, and PMNF as shown in Figures 9 and 10. The temperature and frequency dependence of dielectric loss showed a typical behavior to that of dielectric constant. Also, the value order of samples comes as reported above. The PMF sample showed a value of 1,200 at 303 K, while PMF sample showed a value of 300 at 1 KHz. The low dielectric loss values propose the investigated samples to be good shielding materials.[46] For a more interpretation, the dielectric loss increases with temperature, which is due to the relaxation of charges in cooperation with resulting reduction in the relaxation time; this in turn exerts a double effect on the dielectric loss. On the one hand, the friction between the charges will be increased and then the increase in energy dissipation was observed. On the other hand, the energy required to overcome the internal mechanical friction of the medium will be decreased. Moreover, the dielectric loss decreases with increase in frequency which is due to the high periodic reversal of the field at the interface. The contribution of charges toward the dielectric loss decreases with increase in frequency.

3.8 | Complex impedance

Figure 11 shows the complex impedance of PAn, PMF, PNF, and PMNF at 303 K. As shown, all samples exhibited

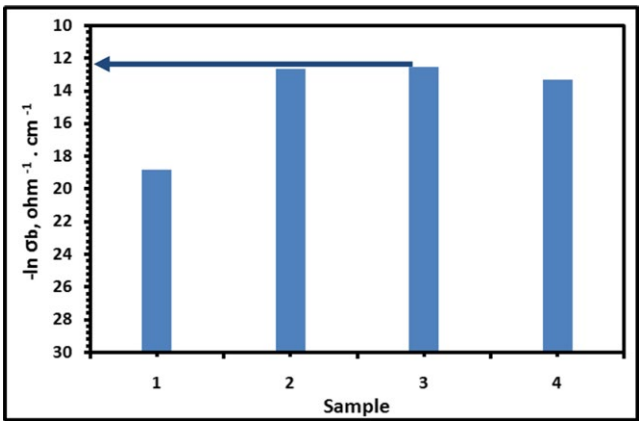

FIGURE 12 Bulk conductivity values of 1: PAn, 2: PMF, 3: PNF and 4: PMNF samples at room temperature (303 K) and a frequency of 100 Hz

a semicircle behavior, indicating the electronic conductivity of PAn and nano ferrite composites.[47] Also, the equivalent circuit was determined from the complex impedance spectrum of each sample, as shown in Figure 11, where R_1 and C_1 are the bulk resistance and capacity of nano ferrite composite, and R_2 is the bulk resistance of electrode–nano ferrite composite interface. To further investigate the bulk electrical properties of all investigated samples, the bulk conductivity was calculated using the equation $\sigma_b = L/R_b A$, where L is the thickness of sample, A is its surface area, and R_b is the bulk resistance (shown as an arrow on the complex impedance figures). All bulk conductivity values are represented in Figure 12. As obviously shown, the PNF sample showed the highest value at room temperature, $\sigma_b = 3.37 \times 10^{-6}$ ohm^{-1} cm^{-1}, while the others showed the following values order: PMF, 3.05×10^{-6} ohm^{-1} cm^{-1} > PMNF, 1.7×10^{-6} ohm^{-1} cm^{-1} > PAn, 6.8×10^{-9} ohm^{-1} cm^{-1}.

3.9 | Magnetic properties

The magnetization (M) versus the applied magnetic field (H) for PAn, PMF, PNF, and PMNF at 303 K is shown in Figure 13. The figure exhibited that all samples have a clear hysteresis behavior. All magnetic parameters (M_s, M_r, H_c) were determined and tabulated in Table 3. According to the literature survey, the pure ferrites have magnetization saturation (M_s) values of 21.33, 39.6, and 34 for $MgFe_2O_4$, $NiFe_2O_4$, and $Mg_{0.5}Ni_{0.5}Fe_2O_4$, respectively.[14,48,49] As shown in Table 3, the magnetization saturation (M_s) values of polymer nano ferrite composites are lower than those of the pure ones. This can be interpreted in a light of the equation, $M_s = \phi\, m_S$, where ϕ is the volume fraction of the particles and m_S is the saturation moment of a single particle. The equation shows that magnetization saturation (M_s) of polymer nano ferrites composites is dependent on the volume fraction (ϕ) of nano ferrite particles in addition to the PAn contribution to the total magnetization.[14] These two parameters will control the magnetic behavior and magnetization parameters. Also, the table showed that nano ferrites addition enhanced the magnetic properties of PAn, except for the PMNF sample that exhibited a low value of magnetization saturation (M_s) compared to the pure PAn one.

TABLE 3 Values of magnetization saturation (M_s), retentivity magnetization (M_r) and coercivity (H_c) of PAn, PMF, PNF and PMNF samples.

Sample	M_s, emu/g	M_r, emu/g	H_C, G
PAn	0.39	87×10^{-3}	329.5
PMF	3.38	16×10^{-2}	88.91
PNF	2.39	47×10^{-2}	298.8
PMNF	0.35	76×10^{-3}	319.23

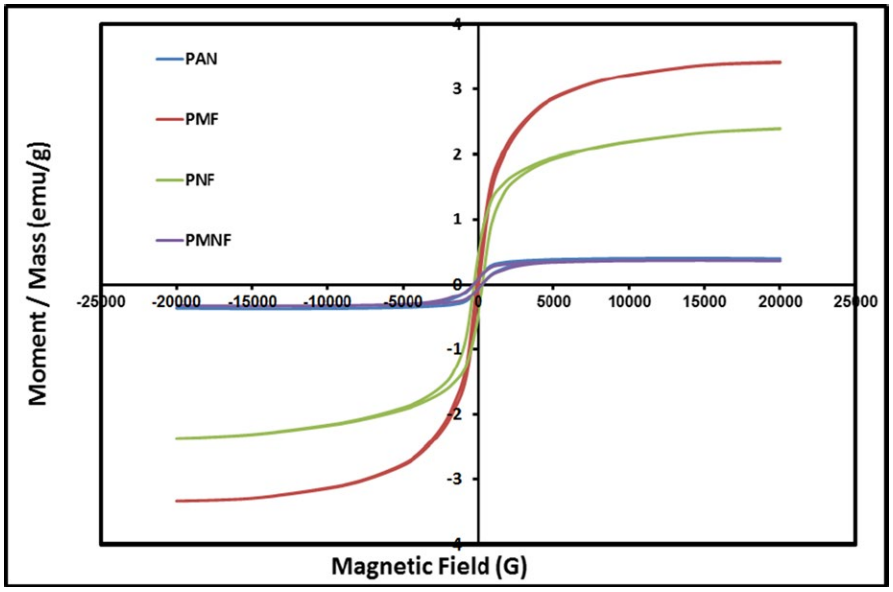

FIGURE 13 Magnetic properties curve of of PAn, PMF, PNF and PMNF samples at room temperature (303 K)

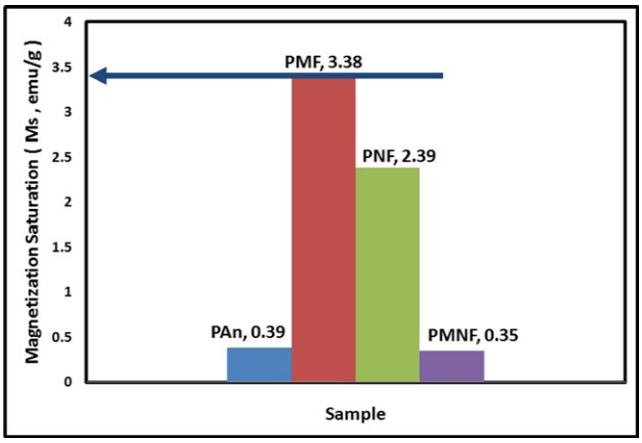

FIGURE 14 Magnetization saturation values of PAn, PMF, PNF and PMNF samples at room temperature (303 K)

In this case and according to what was discussed above (in part of electrical conductivity), this low M_s value of PMNF may be attributed to the unsuitable network formation in presence of $Mg_{0.5}Ni_{0.5}Fe_2O_4$ particles within PAn matrix which may affect the magnetization behavior. This explanation can also be approved through the low magnetization value of pure nickel ferrite particles in presence of PAn–matrix. Pure nickel ferrites have a magnetization saturation value of about 39.6 which exhibits the highest one compared to the other two pure ferrites particles, while exhibits 2.39 in presence of PAn–matrix. At the same time, pure magnesium ferrite particles (which have the lowest magnetization value) showed the highest magnetization value in presence of PAn–matrix (core–shell structure). This means that the interaction nature between ferrite particles and PAn–matrix can determine the magnetization values, because of the additionally generated extended states and charged defects with electronic structures that can be created in presence of Pan–matrix. Here, it is worthwhile to mention that we have two important results: the high magnetization saturation (M_s) values of both the pure PAn and the PMF samples. Also, the pure PAn itself showed a good magnetization saturation value (0.39 emu/g) compared to other synthesized samples in previously reported works.[2,14] This may be attributed to the synthesis method that can introduce more suitable network structure. This can be also supported with a previous work[50]; the properties of polyaniline depend mainly on two important factors: the degree of oxidation and that of protonation. Additionally, the PMF sample having the core–shell structure also exhibited the highest magnetization saturation value ($M_s = 3.38$ emu/g). The other samples showed the following values order: PNF, 2.39 emu/g > PAn, 0.39 emu/g > PMNF, 0.35 emu/g, as shown in Figure 14. To further investigate the effect of small nano ferrite amount (13 wt.%) addition to the pure PAn, a comparison of the optimized sample, PMF, with other previous studies[2,14] containing a high nano ferrite amount (53.7 wt.%) was established. In brief, the sample containing a small nano ferrite amount exhibited a near value of magnetization saturation ($M_s = 3.4$ emu/g) to that containing a high amount ($M_s = 5.9$ emu/g). This indicates that not only the amount can affect the magnetization saturation (M_s) value, but also the nature and degree of interactions with polymer matrix. At the same time, the thermal stability of the PMF sample is good (~500°C) while the similar composite[14] showed a thermal stability value of 590°C. According to these results, this material will have potential applications such as microwave absorption materials, batteries, electrochemical display devices, and electrical–magnetic shields. Finally, we can report that although the presence of a small nano ferrite amount, good properties gotten. This means that if a large one used, better properties expected.

4 | CONCLUSIONS

Polyaniline composites containing small amounts of three different nano ferrites ($MgFe_2O_4$, $NiFe_2O_4$, and $Ni_{0.5}Mg_{0.5}Fe_2O_4$) were synthesized using in situ chemical polymerization method. XRD and FT-IR confirmed the formation of nano composites. Moreover, the different particle shapes produced through the chemical polymerization of each sample were investigated. As an interesting particle shape, PMF sample exhibited the core–shell structure one. This difference may be attributed to the nano ferrite type and the physical interactions nature with polymer matrix. The sample of the core–shell structure, PMF, also showed distinguished magnetic and electrical properties. PMF sample exhibited the highest AC conductivity value (1.01×10^{-4} ohm^{-1} cm^{-1}, at room temperature) compared to the others ones showing the following values order : PMNF, $\sigma_{AC} = 3.72 \times 10^{-5}$ ohm^{-1} c m^{-1} > PNF, $\sigma_{AC} = 1.51 \times 10^{-5}$ ohm^{-1} cm^{-1}. The same sample showed a dielectric constant value of 110, while the others showed the following values order: PMNF, 93.2 > PNF, 35.2 > PAn, 1.2 at 303 K. Also, the bulk conductivity value of PMF sample was of 3.05×10^{-6} ohm^{-1} cm^{-1} at room temperature. Additionally, the PMF sample exhibited the highest magnetization saturation value ($M_s = 3.38$ emu/g). In comparison with other similar composites containing large amounts of the same ferrite, the investigated PMF sample showed good magnetization saturation value and thermal stability behavior. At last, we can conclude that small amounts of ferrites can achieve good properties, especially when good structural interactions exist.

ACKNOWLEDGMENT

The first author (Emad M. Masoud) of this research article would like to thank the financial support of Benha University

(http://www.bu.edu.eg/en/), Egypt, to complete this research work.

ORCID

Emad M. Masoud http://orcid.org/0000-0002-7421-4349

REFERENCES

[1] D. Donescua, R. C. Fierascua, M. Ghiurea, D. M. Maximeanb, C. A. Nicolaea, R. Somoghi, C. I. Spatarua, N. Stanicac, V. Raditoiua, E. Vasile, *Appl. Surf. Sci.* **2017**, *414*, 8.

[2] A. A. Farghali, M. Moussa, M. H. Khedr, *J. Alloys Compd.* **2010**, *499*, 98.

[3] G. Li, S. Yan, E. Zhouc, Y. Chena, *Colloids Surf. A: Physicochem. Eng. Asp.* **2006**, *276*, 40.

[4] F. Xu, L. Ma, Q. Huo, M. Gan, J. Tang, *J. Magn. Magn. Mater.* **2015**, *374*, 311.

[5] O. Kalinina, F. Kumacheva, *Macromolecules* **1999**, *32*, 4122.

[6] G. R. Pedro, *Adv. Mater.* **2001**, *13*, 163.

[7] R. H. Marchessault, P. Rioux, L. Raymond, *Polymer* **1992**, *33*, 4024.

[8] R. F. Ziolo, E. P. Fiannelis, B. A. Weistein, M. P. O'Horo, B. N. Ganguly, V. Mehrotra, M. W. Russell, D. R. Huffman, *Science* **1992**, *257*, 219.

[9] A. Dhanabalan, S. S. Talwar, A. Q. Contractor, N. P. Kumar, S. N. Narang, S. S. Major, K. P. Muthe, J. C. Vyas, *J. Mater. Sci. Lett.* **1999**, *18*, 603.

[10] A. Mirmohseni, A. Oladegaragoze, M. Farbodi, *Iran. Polym. J.* **2008**, *17*, 135.

[11] S. Bhadra, D. Khastgir, N. K. Singha, J. H. Lee, *Prog. Polym. Sci.* **2009**, *34*, 783. https://doi.org/10.1016/j.progpolymsci.2009.04.003.

[12] Z. L. Wang, Y. Liu, Z. Zhang, Handbook of Nanophase and Nanostructured Materials, Vol. *3*, Kluwer Academic/Plenum Publishers, New York **2002**.

[13] S. H. Hosseini, S. H. Mohseni, A. Asadnia, H. Kerdari, *J. Alloys Compd.* **2011**, *509*, 4682.

[14] R. M. Khafagy, *J. Alloys Compd.* **2011**, *509*, 9849.

[15] S. Sultana, K. Z. M. Rafiuddin, K. Umar, *J. Alloys Compd.* **2012**, *535*, 44.

[16] J. Jiang, L. Li, F. Xu, *Mater. Sci. Eng., A* **2007**, *456*, 300.

[17] W. B. Cross, L. Affleck, M. V. Kuznetsov, I. P. Parkin, Q. A. Pankhurst, *J. Mater. Chem.* **1999**, *9*, 2545.

[18] W. E. Mahmoud, H. El-Mallah, *J. Phys. D Appl. Phys.* **2009**, *42*, 035502.

[19] J. P. Pouget, M. E. Jozefowicz, A. J. Epstein, X. Tang, A. G. Macdiarmid, *Macromolecules* **1991**, *24*, 779.

[20] J. Chandradass, M. Balasubramanian, K. H. Kim, *J. Alloys Compd.* **2010**, *506*, 395.

[21] B. A. Bhanvase, N. S. Darda, N. C. Veerkar, A. S. Shende, S. R. Satpute, S. H. Sonawane, *Ultrason. Sonochem.* **2015**, *24*, 87.

[22] J. C. Xu, W. M. Liu, H. L. Li, *Mater. Sci. Eng., C* **2005**, *25*, 444.

[23] S. P. Armes, S. Gottesfeld, J. G. Beery, F. Garzon, S. F. Agnew, *Polymer* **1991**, *32*, 2325.

[24] P. M. Grant, I. P. Batra, *Solid State Commun.* **1979**, *29*, 225.

[25] J. Fink, G. Leising, *Phys. Rev. B* **1986**, *34*, 5320.

[26] P. Dutta, S. Biswas, M. Ghosh, S. K. De, S. Chatterjee, *Synthetic Met.* **2001**, *122*, 455.

[27] S. De, A. Dey, S. K. Dea, *Eur. Phys. J.* **2005**, *46*, 355.

[28] K. C. Kao, W. Hwang, Electrical Transport in Solid, Pergamon Press, Oxford **1981**.

[29] E. M. Masoud, A.-A. El-Bellihi, W. A. Bayoumy, M. A. Mousa, *J. Alloys Compd.* **2013**, *575*, 223.

[30] A. A. ElBellihi, W. A. Bayoumy, E. M. Masoud, M. A. Mousa, *Bull. Korean Soc.* **2012**, *33*, 2949.

[31] E. M. Masoud, A.-A. El-Bellihi, W. A. Bayoumy, M. A. Mousa, *Mater. Res. Bull.* **2013**, *48*, 1148.

[32] E. M. Masoud, *J. Alloys Compd.* **2015**, *651*, 157.

[33] E. M. Masoud, M. E. Hassan, S. E. Wahdaan, S. R. Elsayed, S. A. Elsayed, *Polym. Test.* **2016**, *56*, 277.

[34] E. M. Masoud, A.-A. El-Bellihi, W. A. Bayoumy, E. A. Mohamed, *J. Mol. Liq.* **2018**, *260C*, 237.

[35] E. M. Masoud, M. A. Mousa, *Ionics* **2015**, *21*, 1095.

[36] E. M. Masoud, M. Khairy, M. A. Mousa, *J. Alloys Compd.* **2013**, *569*, 150.

[37] L. Liu, M. Wu, Y. Huang, Z. Yang, L. Fang, C. Hu, *Mater. Chem. Phys.* **2011**, *126*, 769.

[38] L. Liu, H. Fan, L. Fang, H. Dammak, M. Pham-Thi, *J. Electroceram.* **2012**, *28*, 144.

[39] L. Liu, D. Shi, L. Fan, J. Chen, G. Li, L. Fang, B. Elouadi, *J. Mater. Sci. Mater. Electron.* **2015**, *26*, 6592.

[40] X. Sun, J. Deng, S. Liu, T. Yan, B. Peng, W. Jia, Z. Mei, H. Su, L. Fang, L. Liu, *Appl. Phys. A* **2016**, *122*, 864.

[41] Y. Li, L. Fang, L. Liu, Y. Huang, C. Hu, *Mater. Sci. Eng., B* **2012**, *177*, 673.

[42] Y. Huang, D. Shi, L. Liu, G. Li, S. Zheng, L. Fang, *Appl. Phys. A* **2014**, *114*, 891.

[43] M. Wu, L. Fang, L. Liu, G. Li, B. Elouadi, *Ferroelectrics* **2014**, *478*(1), 18.

[44] S. Liu, X. Sun, B. Peng, H. Su, Z. Mei, Y. Huang, J. Deng, C. Su, L. Fang, L. Liu, *J. Electroceram.* **2016**, *37*, 137.

[45] K. Singha, A. Ohlana, R. K. Kotnalab, A. K. Bakhshic, S. K. Dhawan, *Mater. Chem. Phys.* **2008**, *112*, 651.

[46] S. W. Phang, T. Hino, M. H. Abdullah, N. Kuramoto, *Mater. Chem. Phys.* **2007**, *104*, 327.

[47] E. M. Masoud, *Polym. Test.* **2016**, *56*, 65.

[48] K. Nejati, R. Zabihi, *Chem. Cent. J.* **2012**, *6*, 23.

[49] N. M. Deraz, O. H. Abd-Elkader, *Pure Appl. Microbiol.* **2013**, *7*, 333.

[50] J. C. Chiang, A. G. MacDiarmid, *Synthetic Met.* **1986**, *1*, 193.

How to cite this article: Masoud EM, El-Bellihi AA, Bayoumy WA, Abdallah AS. Polymer–spinel ferrite composite containing nickel, magnesium, and nickel–magnesium ions: Structural, magnetic, electrical, and thermal stability properties. *Adv Polym Technol*. 2018;00:1–12. https://doi.org/10.1002/adv.22155